

GASEOUS DYNAMICAL FRICTION IN PRESENCE OF BLACK HOLE RADIATIVE FEEDBACK

KWANGHO PARK AND TAMARA BOGDANOVIĆ

Center for Relativistic Astrophysics, School of Physics, Georgia Institute of Technology, Atlanta, GA 30332, USA
Draft version March 28, 2017

ABSTRACT

Dynamical friction is thought to be a principal mechanism responsible for orbital evolution of massive black holes (MBHs) in the aftermath of galactic mergers and an important channel for formation of gravitationally bound MBH binaries. We use 2D radiative hydrodynamic simulations to investigate the efficiency of dynamical friction in the presence of radiative feedback from an MBH moving through a uniform density gas. We find that ionizing radiation that emerges from the innermost parts of the MBH’s accretion flow strongly affects the dynamical friction wake and renders dynamical friction inefficient for a range of physical scenarios. MBHs in this regime tend to experience positive net acceleration, meaning that they speed up, contrary to the expectations for gaseous dynamical friction in absence of radiative feedback. The magnitude of this acceleration is however negligibly small and should not significantly alter the velocity of MBHs over relevant physical timescales. Our results suggest that suppression of dynamical friction is more severe at the lower mass end of the MBH spectrum which, compounded with inefficiency of the gas drag for lower mass objects in general, implies that $< 10^7 M_{\odot}$ MBHs have fewer means to reach the centers of merged galaxies. These findings provide formulation for a sub-resolution model of dynamical friction in presence of MBH radiative feedback that can be easily implemented in large scale simulations.

Subject headings: accretion, accretion disks – black hole physics – hydrodynamics – radiative transfer

1. INTRODUCTION

A massive perturber moving through some background medium creates in it a density wake. The wake trails the perturber and exerts on it a gravitational force in the direction opposite to the motion, thus acting as a brake and earning this interaction a name: “dynamical friction.” In his seminal work, Chandrasekhar (1943) studied the efficiency of dynamical friction for a massive perturber moving through a stellar background and found the drag force to be maximized when the velocity of the perturber is comparable to the velocity dispersion of stars, $v \approx \sigma$. Ostriker (1999) later evaluated the dynamical friction force acting on a perturber traveling through a uniform gaseous medium and found that the gaseous drag is more efficient than stellar drag for transonic perturbers. This work also established that the gaseous drag is operating most efficiently when $1 < \mathcal{M} \lesssim \text{few}$, where the Mach number $\mathcal{M} \equiv v/c_{s,\infty}$ is defined as the ratio between the perturber velocity v and the sound speed of the ambient gas “at infinity” $c_{s,\infty}$, i.e., in a distant region unaffected by the perturber. In this mildly supersonic regime, the dynamical friction force takes form

$$F_{\text{DF}} = -\frac{4\pi(GM_{\text{BH}})^2\rho_{\infty}}{v^2} \ln \left[\Lambda \left(1 - \frac{1}{\mathcal{M}^2} \right)^{0.5} \right] \quad (1)$$

where M_{BH} is the mass of the perturber (hereafter assumed to be a black hole; BH) and ρ_{∞} is the density of the gas at infinity. $\ln \Lambda = \ln(r_{\text{max}}/r_{\text{min}})$ is the Coulomb logarithm and r_{min} and r_{max} represent the smallest and largest spatial scales in the gas wake that contribute to dynamical friction, respectively. Based on Equation (1), it follows that the effect of dynamical friction is expected

to be stronger for massive perturbers given that they can interact with a sufficiently dense pool of ambient gas.

Because of its efficiency, gaseous drag has been extensively investigated in simulations that follow pairing of massive black holes (MBHs) in gas rich mergers of galaxies (see Mayer 2013, for review). The most important questions for this research area are: in which galaxies does gaseous dynamical friction lead to successful gravitational pairing of MBHs and on what timescales? Calligaris et al. (2009, 2011), for example, find that MBH pairs with mass ratios $q < 0.1$ are less likely to form gravitationally bound binaries within a Hubble time, largely due to the inefficiency of the gas drag on the smaller of the two MBHs. When pairing is successful, gaseous dynamical friction is capable of transporting the MBHs from galactic radii of a few hundred to ~ 1 pc on timescales as short as $\sim 10^7$ year and tens of times faster than stellar dynamical friction (for e.g., Escala et al. 2005; Dotti et al. 2006; Mayer et al. 2007).

Interestingly, gravitational interaction of the MBH with the surrounding gas is quite local. For example, for a BH with mass $\sim 10^6 M_{\odot}$ most of the gravitational drag force is contributed by the gas that resides within only a few parsecs of the MBH (Chapon et al. 2013). This proximity implies that the dynamical friction wake can be strongly affected, and possibly obliterated, by irradiation and feedback from an accreting MBH. Indeed, studies of dynamical evolution of MBHs find that dynamical friction can be significantly reduced due to the wake dispersal caused by purely thermal feedback from MBHs in simulations that follow gravitationally recoiled MBHs (Sijacki et al. 2011) and BH pairing (Souza Lima et al. 2016) where the term “wake evacuation” is dubbed. These results bring into question the assumed efficacy of gaseous dynamical friction and call for further exploration of the effects of radiative feedback powered by

MBH accretion.

Here, we investigate this question by considering interaction of matter and radiation in the gravitational potential well of a moving MBH. The most important findings of this work are that there are regimes, set by the properties of the MBH and its ambient medium, in which gas dynamical friction is rendered inefficient by the MBH feedback. We lay out the relevant physical regimes and scales in Section 2 and evaluate the efficiency of dynamical friction using local radiation hydrodynamic simulations in Section 3. We discuss implications of our findings and conclude in Section 4.

2. REGIMES OF DYNAMICAL FRICTION IN THE PRESENCE OF RADIATIVE FEEDBACK

Photoionization and radiation pressure exerted by radiation escaping from the innermost parts of the BH accretion flow can create the ionized region (the Strömgren sphere or H II region) around the a BH and strongly alter the properties of surrounding gas. This radiation “response”, also referred to as the BH radiative feedback, has been found to lower the accretion rate by orders of magnitude relative to a fiducial case in which radiative feedback is neglected (Milosavljević et al. 2009; Li 2011; Park & Ricotti 2011, 2012; Pacucci & Ferrara 2015; Park et al. 2016). In the context of dynamical friction, this accretion regime is also likely to correspond to reduced efficiency of the gas drag due to the impact of ionizing radiation on the BH’s density wake.

Park et al. (2014a) and Inayoshi et al. (2016) however find a physical regime at higher gas densities in which the nature of accretion onto the BH fundamentally changes from this picture, as the H II region collapses under the gravity of the surrounding gas, and accretion continues unaffected by radiation at supper Eddington rates. The two studies differ in their treatment of radiation transport: the latter considers the effects of radiation trapping at high accretion rates (Begelman 1978, 1979) while the former neglects them. Both nevertheless indicate that conditions for hyper-accretion arise for a BH immersed in neutral gas with number density n_∞ , when $n_\infty M_{\text{BH}} > 10^9 - 10^{10} M_\odot \text{cm}^{-3}$. This finding implies that the density distribution of gas in the hyper-accretion regime is only weakly affected by radiation pressure, and thus the efficiency of dynamical friction is likely to be restored to that predicted classically, i.e., in absence of radiative feedback.

For moving BHs, accretion rate, and thus accretion luminosity, also depend on BH velocity. We draw on the results of Park & Ricotti (2013, hereafter PR13), who used radiation hydrodynamic simulations to investigate the growth and luminosity of BHs moving through a uniform gaseous medium with temperature $T_\infty = 10^4 \text{K}$. PR13 show that in this case the BH radiative feedback causes a formation of an H II region elongated along the direction of the BH motion and filled with ionized hydrogen (or H–He) gas of temperature, $T_{\text{in}} \approx 4 \times 10^4 \text{K}$ ($6 \times 10^4 \text{K}$). A shell of gas with increased density, corresponding to $(1 + \mathcal{M}^2)n_\infty$, forms in front of the BH as a consequence of the “snowplow” effect caused by radiation pressure. For a wide range of simulated gas densities the shell becomes gravitationally unstable and collapses when $\mathcal{M} \gtrsim 4$, restoring the properties of the gas flow around the BH to the classical Bondi–Hoyle–Lyttleton

solution (Hoyle & Lyttleton 1939; Bondi & Hoyle 1944). While PR13 have not explicitly investigated the properties of the gas wake in their simulations, it follows that in this regime the efficiency of dynamical friction is restored to its classically derived value.

We therefore focus on scenarios described by $1 \leq \mathcal{M} < 4$, when gas dynamical friction is classically expected to be most efficient, and $(1 + \mathcal{M}^2) M_{\text{BH}} n_\infty < 10^9 M_\odot \text{cm}^{-3}$, when the influence of the BH radiative feedback on dynamical friction wake is expected to be significant. Having established the relevant regime we estimate the extent of the dynamical friction wake and compare it to the size of the H II region.

2.1. Relevant scales

The extent of the dynamical friction wake that would form behind the MBH in absence of radiative feedback can be estimated as a radius of the gravitational influence of the MBH

$$R_{\text{DF}} \approx \frac{GM_{\text{BH}}}{c_{s,\infty}^2} = 52.1 \text{ pc} \left(\frac{T_\infty}{10^4 \text{ K}} \right)^{-1} \left(\frac{M_{\text{BH}}}{10^6 M_\odot} \right). \quad (2)$$

Here $c_{s,\infty} = \sqrt{\gamma k_B T_\infty / \mu m_p} = 9.1 \text{ km s}^{-1} (T_\infty / 10^4 \text{ K})^{1/2}$, assuming isothermal gas with hydrogen composition characterized by the adiabatic index $\gamma = 1$ and mean atomic weight $\mu = 1$. The constants have their usual meaning. As mentioned in Section 1, most of the gravitational drag force is contributed by the gas that resides within an order of magnitude smaller region than that estimated in equation (2), so this value can be considered a conservative upper limit.

The size of the elongated H II region sensitively depends on the MBH accretion rate and velocity. For the purpose of the estimates presented here, we neglect the elongation of the H II region and estimate the radius of a spherically symmetric ionization sphere that would form around a stationary MBH accreting hydrogen gas, $R_{\text{HII}} = (3\dot{N}/4\pi\alpha_{\text{rec}})^{1/3} n_\infty^{-2/3}$ (Osterbrock & Ferland 2006). The number of ionizing photons per unit time emitted from the innermost parts of a BH’s accretion flow is

$$\dot{N} = \int_{\nu_0}^{\infty} \frac{L_\nu}{h\nu} d\nu \approx \frac{\alpha - 1}{\alpha} \left(\frac{L_{\text{bol}}}{h\nu_0} \right) \quad (3)$$

which is characterized by bolometric luminosity $L_{\text{bol}} = \int_0^\infty L_\nu d\nu$ and $L_\nu \propto \nu^{-\alpha}$. Here, $\alpha = 1.5$ is the spectroscopic index representative of the spectral energy distribution (SED) of active galactic nuclei (AGN) in the high accretion state, and $h\nu_0 = 13.6 \text{ eV}$ for hydrogen. $\alpha_{\text{rec}} = 4 \times 10^{-13} \text{ cm}^3 \text{ s}^{-1}$ corresponds to the Case A recombination coefficient for hydrogen gas at the temperature $T_\infty = 10^4 \text{ K}$, used here so to match simulations described in the next section. Note that the Case B coefficient is a more appropriate choice for the high gas densities in this problem, which would result in a small change Strömgren radius being proportional to $\alpha_{\text{rec}}^{-1/3}$. We consider accretion powered BH luminosity, $L_{\text{bol}} = \eta \dot{M} c^2$, and assume radiative efficiency $\eta = 0.1$ (Shakura & Sunyaev 1973).

These ingredients provide an estimate for the size of the H II region, given a known MBH accretion rate. In the case of moving MBHs with the Mach number in the

TABLE 1
SIMULATION PARAMETERS

ID	$N_r \times N_\theta$	$\Delta r/r$	\mathcal{M}	t_{end} (Myr)
HR	400×128	0.026	0.5, 1.0, 2.0	201.0, 74.9, 74.9
MR	300×96	0.035	0.5, 1.0, 2.0	201.0, 201.0, 201.0
LR	200×64	0.053	0.5, 1.0, 1.5, 2.0	201.0, 201.0, 201.0, 201.0

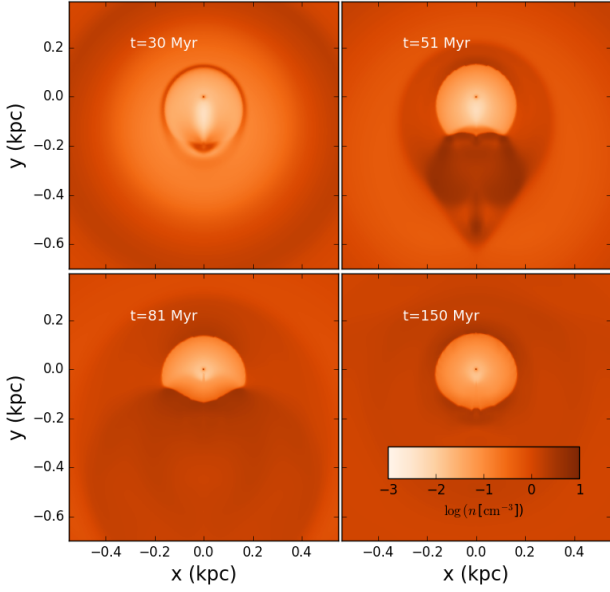


FIG. 1.— Snapshots of gas number density at different times for the HR run with $\mathcal{M} = 0.5$. The flow of gas is from top to bottom and the BH is located at $(x, y) = (0, 0)$ in each panel. The shape of the H II region and dynamical friction wake reach steady state after 150 Myr in this simulation.

range $1 < \mathcal{M} < 4$, PR13 find that the accretion rate mediated by radiation feedback can be expressed as

$$\dot{M} \approx 1.2 \times 10^{-2} \mathcal{M}^2 \dot{M}_B \left(\frac{T_\infty}{T_{\text{in}}} \right)^{5/2} \quad (4)$$

where \dot{M}_B is the nominal Bondi accretion rate for isothermal gas (Bondi & Hoyle 1944)

$$\begin{aligned} \dot{M}_B &= \frac{\pi e^{3/2} \rho_\infty (GM_{\text{BH}})^2}{c_{s,\infty}^3} \\ &= 8.7 \times 10^{-3} \left(\frac{n_\infty}{1 \text{ cm}^{-3}} \right) \left(\frac{T_\infty}{10^4 \text{ K}} \right)^{-3/2} \left(\frac{M_{\text{BH}}}{10^6 M_\odot} \right)^2 M_\odot \text{ yr}^{-1}. \end{aligned} \quad (5)$$

Combining Equations (3)–(5), we obtain the estimate for the radius of the H II sphere

$$R_{\text{HII}} \approx 430 \text{ pc } \mathcal{M}^{2/3} \left(\frac{n_\infty}{1 \text{ cm}^{-3}} \right)^{-1/3} \left(\frac{T_{\text{in}}}{4 \times 10^4 \text{ K}} \right)^{-1/2} \left(\frac{M_{\text{BH}}}{10^6 M_\odot} \right)^{2/3}. \quad (6)$$

Considering the ratio of Equations (6) and (2) we get

$$\frac{R_{\text{HII}}}{R_{\text{DF}}} \sim 8 \mathcal{M}^{2/3} \left(\frac{T_\infty}{10^4 \text{ K}} \right) \left(\frac{T_{\text{in}}}{4 \times 10^4 \text{ K}} \right)^{-1/2} \left(\frac{M_{\text{BH}} n_\infty}{10^6 M_\odot \text{ cm}^{-3}} \right)^{-1/3} \quad (7)$$

where we find that $R_{\text{HII}} \gtrsim R_{\text{DF}}$ for all values of the Mach number in the range $1 < \mathcal{M} < 4$ and when

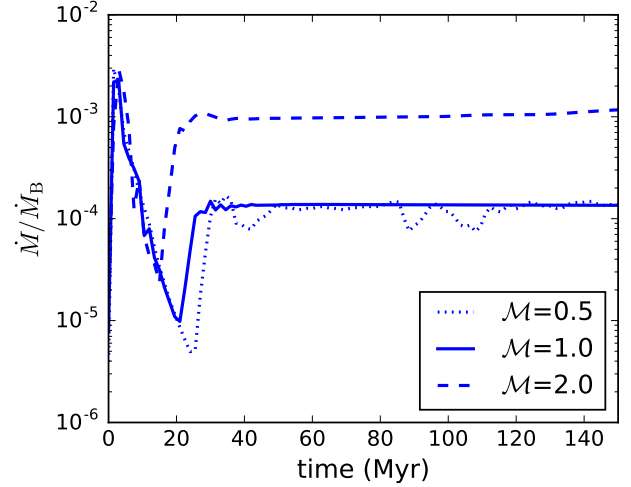


FIG. 2.— Accretion rate onto the MBH as a function of time shown in units of Bondi accretion rate defined in Equation (5). Different line styles mark MR runs with $\mathcal{M} = 0.5, 1.0, \text{ and } 2.0$.

$(1 + \mathcal{M}^2) M_{\text{BH}} n_\infty < 10^9 M_\odot \text{ cm}^{-3}$. It follows that in this regime the dynamical friction wake is likely to be fully ionized and dispersed by the MBH radiative feedback, especially given the proximity of the wake mentioned before.

In the next section we examine the detailed structure of the wake and the H II region, and numerically evaluate the resulting dynamical friction force from radiation hydrodynamic simulations.

3. RADIATION-HYDRODYNAMIC SIMULATIONS

3.1. Numerical Setup

We run a set of 2D radiation hydrodynamic simulations using a parallel version of the non-relativistic code ZEUS-MP (Stone & Norman 1992; Hayes et al. 2006). Simulations are carried out in a polar coordinate system defined by coordinates (r, θ) and assuming axisymmetry with respect to the MBH’s direction of motion. The extent of the computational domain is given by $r \in (0.1 \text{ pc}, 3.0 \text{ kpc})$ and $\theta \in (0, \pi)$ and other relevant quantities are shown in Table 1. In the calculation of gas dynamics we consider only the gravitational potential of the MBH and neglect the self-gravity of the gas.

An MBH with mass $M_{\text{BH}} = 10^6 M_\odot$, located at the origin of the coordinate system ($r = 0$), is placed in a “wind tunnel.” In this setup, the gas of uniform density $n_\infty = 1.0 \text{ cm}^{-3}$ and temperature $T_\infty = 10^4 \text{ K}$ is assumed to flow into the computational domain in direction $\theta = \pi$. We evaluate the accretion rate onto the MBH by calculating the mass flux through the inner boundary of the computational domain, defined by the sphere with radius $r_{\text{min}} = 0.1 \text{ pc}$, and convert it to MBH luminosity as $L_{\text{bol}} = 0.1 \dot{M} c^2$. The SED of ionizing radiation is described as $L_\nu \propto \nu^{-1.5}$ using 50 energy bins ranging

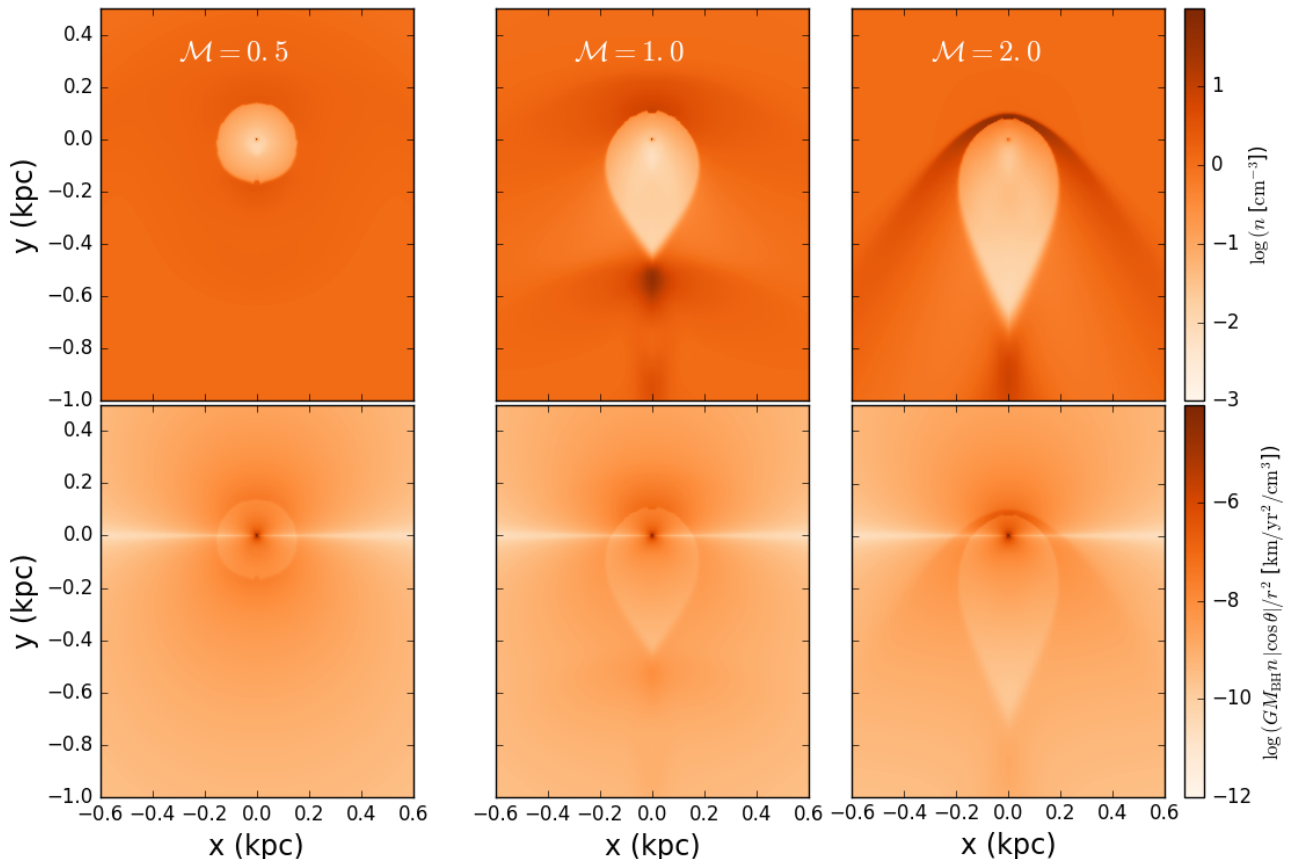


FIG. 3.— Top: 2D snapshots of the number density of gas at $t = 150$ Myr for MR runs $\mathcal{M} = 0.5, 1.0,$ and 2.0 (left to right). All snapshots show steady state gas distributions. Bottom: contribution to dynamical friction from the gas surrounding the MBH, evaluated as the gravitational acceleration per unit volume along the direction of the MBH motion.

from 13.6 eV to 100 keV.

The composition of the H–He gas is evolved by following the species of H I, H II, He I, He II, He III, and e^- . The radiation transport is coupled with hydrodynamics and includes photo-heating, photo-ionization, Compton heating by UV and X-ray photons from the BH, and gas cooling (Park & Ricotti 2011, 2012; Park et al. 2014a,b). We assume that BH radiation is the only heating source and adopt a simple analytic form of atomic cooling function $\Lambda(T)$ due to neutral and ionized H and He, which includes cooling by recombination, collisional ionization/excitation, free-free transitions, and dielectric recombination of He II (Shapiro & Kang 1987). Molecular cooling is neglected and the cooling rate is set to zero below $T = 10^4$ K. The calculation of radiation transfer accounts for the radiation pressure and thus allows us to accurately capture the effects of both energy and momentum feedback (see Park & Ricotti 2012, for implementation details). Hydrodynamic and radiative transfer equations are solved at every time step defined as $\Delta t = \min(\Delta_{\text{hydro}}, \Delta_{\text{chem}})$, where Δ_{hydro} is the hydrodynamical time step and Δ_{chem} is the time step required to calculate the change of chemical abundances (Ricotti et al. 2001; Whalen & Norman 2006).

We investigate the effect of radiative feedback on the dynamical friction wake by varying the MBH Mach number from 0.5 (subsonic) to 2.0 (supersonic), while keep-

ing M_{BH} , n_∞ , and T_∞ fixed. Each simulation is run for several sound crossing timescales, defined as $t_{\text{cross}} = R_{\text{HII}}/c_{s,\infty}$, which corresponds to 46 Myr for the size of the H II region defined by equation (6). This ensures that the accretion rate onto the MBH and density distribution of the gas in the dynamical friction wake reach steady state. The length of each simulation is recorded as t_{end} in Table 1. We test numerical convergence with the set of high (HR), medium (MR), and low resolution (LR) runs. The HR runs are carried out with resolution of $(N_r \times N_\theta) = (400 \times 128)$, MR with (300×96) , and LR with (200×64) . The radial bins are logarithmically spaced so that $\Delta r/r$ is constant everywhere on the grid while the bins in polar angle are evenly spaced and have size $\Delta\theta = \pi/N_\theta$. The outer boundary of the computational domain is defined as inflow where $0 \leq \theta \leq \pi/2$ and outflow for $\pi/2 < \theta \leq \pi$. We apply the outflow boundary conditions at the inner domain boundary.

3.2. Evolution of the H II region and overdensity wake

The snapshots in Figure 1 illustrate the evolution of the gas density in the HR run with $\mathcal{M} = 0.5$. A low density H II region with $T_{\text{in}} \approx 6 \times 10^4$ K forms promptly around the MBH, while the distribution of gas outside of it reaches steady state 150 Myr after the beginning of the simulation. This timescale is consistent with ~ 7 sound crossing times for the H II region of the size 200 pc.

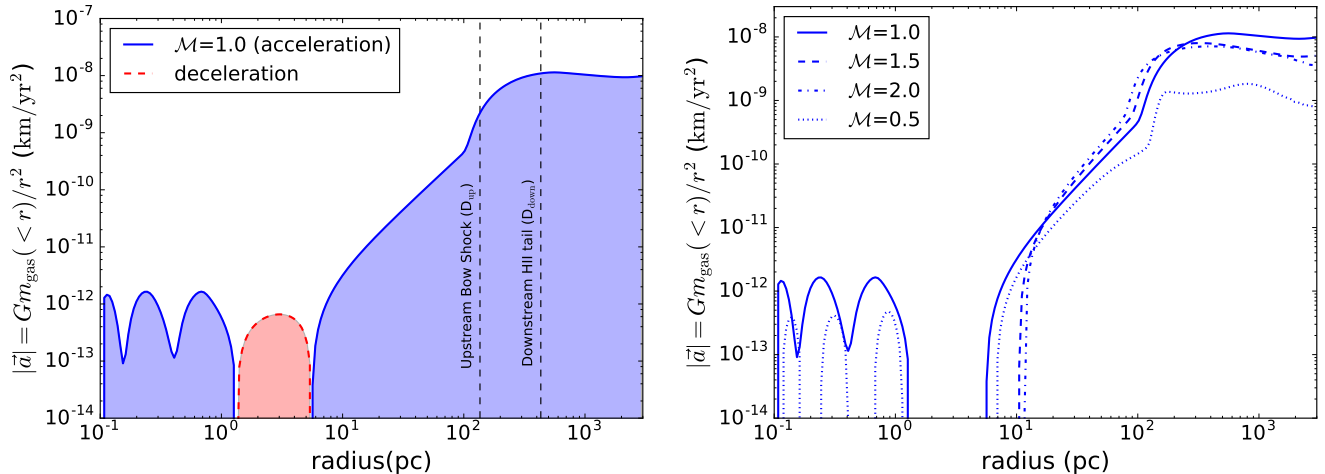


FIG. 4.— Left: magnitude of the MBH acceleration along the direction of motion (either positive or negative) contributed by the gas within polar radius r for the LR $\mathcal{M} = 1.0$ run. The MBH is located at the origin $r = 0$. Dashed lines mark the locations of the upstream bow shock and the tail of the downstream H II region, respectively. Right: magnitude of the positive component of acceleration (resulting in MBH speed-up) contributed by the gas within r . Different lines mark LR runs with $\mathcal{M} = 0.5, 1.0, 1.5,$ and 2.0 .

Once steady state is achieved, the shape of the H II region shows minor deviation from spherical symmetry.

Figure 2 shows the accretion rate as a function of time for the MR runs with $\mathcal{M} = 0.5, 1.0,$ and 2.0 . In all simulations MBH initially exhibits a relatively high accretion rate, which decreases as the H II region expands into the background medium as a consequence of the MBH radiative feedback. The expansion of the H II sphere is brought to a halt at $\sim 15 - 30$ Myr after the beginning of the simulation, at which point the accretion rate reaches a turning (minimum) point and readjusts to a steady state value after $\sim 20 - 35$ Myr. This happens first in the LR run with $\mathcal{M} = 2.0$, followed by $\mathcal{M} = 1.0$ and 0.5 . This hierarchy of timescales is determined by the inflow rate of the gas into the H II region as seen by the MBH.

Figure 2 also illustrates the dependence $\dot{M} \propto \mathcal{M}^2$ captured by Equation (4) and applicable in the range $1 < \mathcal{M} < 4$. This dependence of accretion rate on the Mach number was first reported by PR13, who noted that accretion onto the MBH is mediated by a dense shell, which forms upstream from the MBH, at the interface of the H II region and ambient gas. This dense shell and the associated bow shock are discernible in Figure 3, in the MR runs with $\mathcal{M} = 1.0$ and 2.0 , and are absent for the subsonic run with $\mathcal{M} = 0.5$. The same figure shows that the H II region becomes more elongated in the direction of the MBH motion with the increasing Mach number, engulfing a larger volume in the region where the dynamical friction wake is supposed to form. Despite this effect, a noticeable overdensity of gas persists at the tail of the H II region in all simulations, indicating that some fraction of the dynamical friction wake remains present.

The bottom panels of Figure 3 illustrate the strength of gravitational interaction between the MBH and fluid elements in the computational domain, where we evaluate the magnitude of the acceleration per unit volume along the direction of the BH motion as $GM_{\text{BH}} n |\cos \theta| / r^2$. The net effect of a given fluid element on the MBH depends on its location. The gas in the upstream ($0 \leq \theta \leq \pi/2$) acts to accelerate the MBH, while the gas in the

downstream ($\pi/2 \leq \theta \leq \pi$) decelerates it. The shade of the color indicates that the MBH most strongly interacts with the gas in its immediate vicinity, within a radius of a few parsecs, but this distribution appears front-back symmetric and is thus not expected to significantly contribute to the acceleration of the MBH. Similarly, the fluid elements perpendicular to the MBH's line of motion at $\theta \approx \pi/2$ make a negligible contribution. The overdensity of gas that forms at the front and tail of the H II region is thus expected to contribute to the net acceleration of the MBH. In the run with $\mathcal{M} = 0.5$ this distribution is approximately front-back symmetric, indicating a lower magnitude of acceleration. The $\mathcal{M} = 1.0$ and 2.0 runs, on the other hand, show enhanced contribution to MBH acceleration from the front of the H II region, while contribution from the tail appears less significant. In order to determine whether the MBH accelerates or decelerates, once the steady state distribution of gas is achieved, we integrate contributions to the dynamical friction force from all fluid elements in the computational domain.

3.3. Efficiency of dynamical friction

The left panel of Figure 4 shows the steady state magnitude of the MBH acceleration (either positive or negative) due to the gas enclosed within the sphere of radius r for the LR run with $\mathcal{M} = 1.0$. Positive acceleration is defined to be in the direction of the MBH motion, thus resulting in the speed-up of the MBH. Note that the assumption of azimuthal symmetry guarantees that the components of acceleration perpendicular to the MBH's line of motion cancel out, leaving the parallel components as the only contribution.

The magnitude of acceleration is relatively low in the immediate vicinity of the MBH ($r < 3$ pc), consistent with the earlier observation of the front-back symmetry in this region. At $r \gtrsim 3$ pc the magnitude of acceleration gradually increases as the contrast between the upstream and downstream distribution of gas increases with radius. At $r \approx 100$ pc, acceleration shows a sudden jump coinciding with the upstream overdensity and associated bow shock. The acceleration magnitude levels off

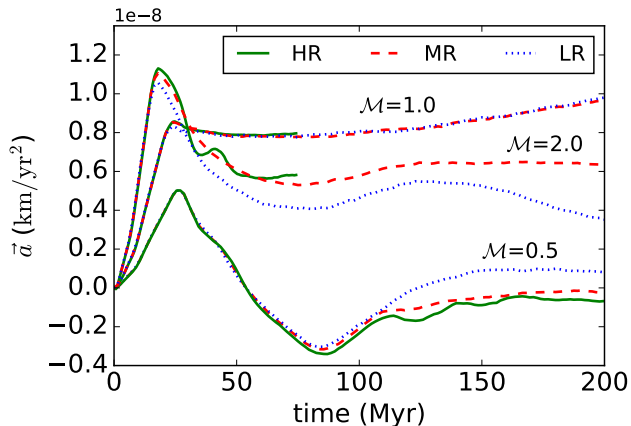


FIG. 5.— Evolution of the net acceleration, integrated over the entire computational domain, for the HR (solid lines), MR (dashed), and LR (dotted) runs with $\mathcal{M} = 0.5, 1.0,$ and 2.0 . Positive acceleration implies speed-up of the MBH.

beyond 400 pc, which marks the spatial extent of the tail of the H II sphere. Evidently, the dynamical friction wake does not contribute to the MBH acceleration beyond this point.

The right panel of Figure 4 shows the magnitude of the positive component of MBH acceleration contributed by the gas enclosed within radius r . The figure illustrates that in all simulations the largest contribution to the MBH acceleration originates from the region $r \gtrsim 10$ pc. This acceleration is net positive, thus speeding up the MBH. In all cases, the MBH deceleration due to the wake beyond the tail of the H II region is negligible. The acceleration originating from $r < 10$ pc can be either positive or negative but is orders of magnitude smaller relative to the larger spatial scales and can be neglected.

Figure 5 shows the evolution of the net acceleration integrated over the entire computational domain as a function of time. In all cases acceleration initially peaks at 15–30 Myrs. This is the same point in time where the accretion rate reaches minimum (Figure 2), indicating a buildup of the dense shell of gas in the upstream of the MBH, which exerts gravitational influence and initially suppresses accretion onto the MBH. Gravitational influence of the upstream gas shell is counterbalanced by the gas in the downstream of the MBH, where overdensity wake develops with a delay corresponding to a few sound crossing times across the elongated H II region. Consequently, the MBH acceleration reaches steady state with a delay of ~ 150 Myr, long after the accretion rate has settled into steady state. An inspection of Figure 5 shows that the net acceleration for the scenario $\mathcal{M} = 1.0$ continues to gently increase even after 200 Myr.

For $\mathcal{M} = 1.0$ and 2.0 the net end value of acceleration is positive, indicating a speed-up of the MBH. As expected, the magnitude of acceleration is smallest for the $\mathcal{M} = 0.5$ scenario, where the gas flow around the MBH exhibits a large degree of front-back symmetry. Figure 5 illustrates that the sign of net acceleration in this case is resolution dependent, where the final outcome of the LR run is MBH speed-up and in the MR and HR runs, deceleration. The net accelerations in the MR and HR runs track each other closely and differ by only $\sim 0.05 \text{ km yr}^{-2}$, indicating numerical convergence of the MR run. We therefore use this value as a measure

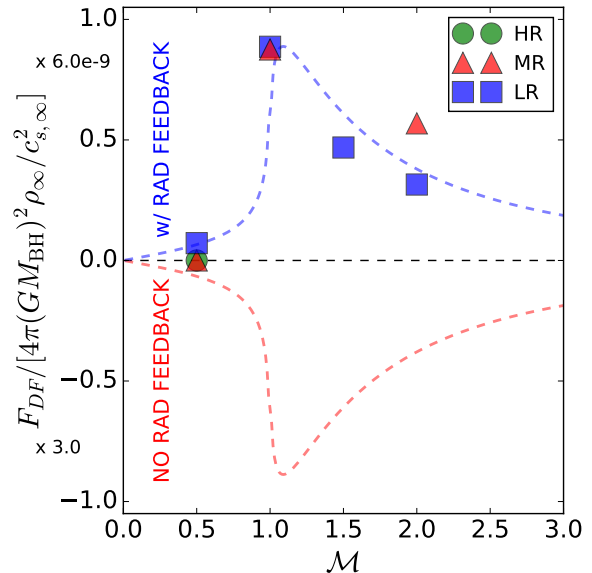


FIG. 6.— Dynamical friction force as a function of the Mach number. The red dashed line illustrates the magnitude of the dynamical friction force in the absence of radiative feedback as calculated by Ostriker (1999). The blue dashed line is the same as the red one but plotted with a positive sign and arbitrarily scaled in magnitude to match data points. Different symbols mark results of the runs with radiative feedback at $t = 201.0$ Myr. Note the different magnitudes of the positive and negative y -axis.

of error in net acceleration due to the finite numerical resolution of our simulations.

Figure 6 shows the values of the dynamical friction force measured at the end of each simulation for different values of \mathcal{M} . As a comparison, the red dashed line shows the dynamical friction force in the absence of radiative feedback, as predicted by Ostriker (1999) for $\ln(c_{s,\infty}t/r_{\min}) = 4$. As noted before, the dynamical friction force calculated from simulations presented in this study is net positive for $1.0 \leq \mathcal{M} < 4$ and negative for $\mathcal{M} = 0.5$. The magnitude of this force is however over ~ 9 orders of magnitude lower compared to that experienced by the MBHs in absence of radiative feedback and is therefore negligible for all values of the Mach number $\mathcal{M} < 4$. Interestingly, the dynamical friction force in the presence of radiative feedback appears to mirror its classical counterpart: it peaks around $\mathcal{M} \approx 1$ and decreases at larger values of the Mach number.

4. DISCUSSION AND CONCLUSIONS

We investigate the efficiency of dynamical friction in presence of radiative feedback from an MBH moving through a uniform density gas. Ionizing radiation that emerges from the innermost parts of the MBH's accretion flow results in the formation of the H II region, which strongly affects the dynamical friction wake and renders dynamical friction inefficient for a range of physical scenarios. We summarize our main findings below:

- We identify a physical regime in which the dynamical friction wake is likely to be fully ionized and dispersed by the MBH radiative feedback as a regime in which the radius of the H II sphere is larger than the extent of the dynamical friction wake. This condition is fulfilled when $\mathcal{M} < 4$

and $(1 + \mathcal{M}^2) M_{\text{BH}} n_{\infty} < 10^9 M_{\odot} \text{cm}^{-3}$. Outside of this regime the formation of the H II region is suppressed and the properties of the gas flow around the MBH are restored to the classical Bondi–Hoyle–Lyttleton solution, thus restoring the effect of dynamical friction. These criteria can be utilized as a sub-resolution model for dynamical friction in large scale simulations that do not resolve the scale of the H II region or MBH density wake.

- Based on radiation hydrodynamic simulations we find that the net acceleration experienced by the MBHs in this regime tends to be positive, meaning that they speed up, contrary to the expectations for gaseous dynamical friction in absence of radiative feedback. This reversal happens because the dominant contribution to the MBH acceleration comes from the dense shell of gas that forms in front of the MBH as a consequence of the snowplow effect caused by radiation pressure.
- The magnitude of MBH acceleration peaks at $\mathcal{M} \approx 1$ and decreases for larger values of the Mach number, similar to the dynamical friction force in absence of radiative feedback. The magnitude of acceleration is however negligibly small, implying that MBHs in this regime will not significantly change their velocity over timescales that determine their motion and properties of their environment.
- Our results suggest that suppression of dynamical friction by radiative feedback should be more severe at the lower mass end of the MBH spectrum, because these BHs must reside in regions of relatively high gas density in order to experience efficient dynamical friction in the regime when $(1 + \mathcal{M}^2) M_{\text{BH}} n_{\infty} > 10^9 M_{\odot} \text{cm}^{-3}$. Compounded with inefficiency of the gas drag for lower mass objects in general this implies that $< 10^7 M_{\odot}$ MBHs have fewer means to reach the centers of merged galaxies.

This study makes several idealized assumptions, such as the uniform gas density and infinite background medium. In reality however, MBHs in the aftermath of galactic mergers are likely to find themselves immersed

in inhomogeneous and clumpy medium which can perturb their otherwise smooth orbital decay (Fiacconi et al. 2013). Furthermore, the geometry and properties of the H II region will be affected in scenarios where the H II region is not confined by the gaseous medium. An example of this would be an H II region around the MBH orbiting within the galactic gas disk. When the radius of the H II region exceeds the half thickness of the disk, the radiation can escape outside of the disk plane, making the problem fully three-dimensional. Even in such scenarios, the proximity of the dynamical friction wake to the MBH is likely to result in the wake obliteration by high energy radiation. Indeed, 3D hydrodynamic simulations that capture the dynamics of MBHs in proper galactic setups also find a weakening of the dynamical friction force in the presence of MBH feedback (Sijacki et al. 2011; Souza Lima et al. 2016). The high resolution, local simulations presented here support these findings and provide a set of criteria, formulated in terms of the properties of the gas and MBH, under which the wake evacuation is efficient.

Along similar lines, we consider an isolated MBH on a linear trajectory, whereas the front–back asymmetry of the density wake for a perturber on a circular orbit has been shown to cause small differences in the dynamical friction force in absence of radiative feedback (Kim & Kim 2007). A system consisting of multiple MBHs would further add to the complexity in cases when dynamical friction wakes can mutually affect one another (e.g., Kim et al. 2008). This type of study may require a transition from 2D to 3D simulations in the future in order to relax the assumption of azimuthal symmetry and properly capture the interplay of inhomogeneities, radiative feedback, and dynamical friction.

This work is supported in part by the National Science Foundation under the Theoretical and Computational Astrophysics Network (TCAN) grant AST-1333360. T.B. acknowledges support from the Research Corporation for Science Advancement through a Cottrell Scholar Award. T.B. is a member of the MAGNA project (<http://www.issibern.ch/teams/agnactivity>) supported by the International Space Science Institute (ISSI) in Bern, Switzerland. Numerical simulations presented in this paper were performed using the high-performance computing cluster PACE, administered by the Office of Information and Technology at the Georgia Institute of Technology.

REFERENCES

- Begelman, M. C. 1978, *MNRAS*, 184, 53
 —. 1979, *MNRAS*, 187, 237
 Bondi, H., & Hoyle, F. 1944, *MNRAS*, 104, 273
 Callegari, S., Kazantzidis, S., Mayer, L., et al. 2011, *ApJ*, 729, 85
 Callegari, S., Mayer, L., Kazantzidis, S., et al. 2009, *ApJ*, 696, L89
 Chandrasekhar, S. 1943, *ApJ*, 97, 255
 Chapon, D., Mayer, L., & Teyssier, R. 2013, *MNRAS*, 429, 3114
 Dotti, M., Colpi, M., & Haardt, F. 2006, *MNRAS*, 367, 103
 Escala, A., Larson, R. B., Coppi, P. S., & Mardones, D. 2005, *ApJ*, 630, 152
 Fiacconi, D., Mayer, L., Roškar, R., & Colpi, M. 2013, *ApJ*, 777, L14
 Hayes, J. C., Norman, M. L., Fiedler, R. A., et al. 2006, *ApJS*, 165, 188
 Hoyle, F., & Lyttleton, R. A. 1939, in *Proceedings of the Cambridge Philosophical Society*, Vol. 35, *Proceedings of the Cambridge Philosophical Society*, 405–+
- Inayoshi, K., Haiman, Z., & Ostriker, J. P. 2016, *MNRAS*, 459, 3738
 Kim, H., & Kim, W.-T. 2007, *ApJ*, 665, 432
 Kim, H., Kim, W.-T., & Sánchez-Salcedo, F. J. 2008, *ApJ*, 679, L33
 Li, Y. 2011, *ArXiv e-prints*, arXiv:1109.3442
 Mayer, L. 2013, *Classical and Quantum Gravity*, 30, 244008
 Mayer, L., Kazantzidis, S., Madau, P., et al. 2007, *Science*, 316, 1874
 Milosavljević, M., Couch, S. M., & Bromm, V. 2009, *ApJ*, 696, L146
 Osterbrock, D. E., & Ferland, G. J. 2006, *Astrophysics of gaseous nebulae and active galactic nuclei*
 Ostriker, E. C. 1999, *ApJ*, 513, 252
 Pacucci, F., & Ferrara, A. 2015, *MNRAS*, 448, 104
 Park, K., & Ricotti, M. 2011, *ApJ*, 739, 2
 —. 2012, *ApJ*, 747, 9

- . 2013, *ApJ*, 767, 163
- Park, K., Ricotti, M., Di Matteo, T., & Reynolds, C. S. 2014a, *MNRAS*, 437, 2856
- . 2014b, *MNRAS*, 445, 2325
- Park, K., Ricotti, M., Natarajan, P., Bogdanović, T., & Wise, J. H. 2016, *ApJ*, 818, 184
- Ricotti, M., Gnedin, N. Y., & Shull, J. M. 2001, *ApJ*, 560, 580
- Shakura, N. I., & Sunyaev, R. A. 1973, *A&A*, 24, 337
- Shapiro, P. R., & Kang, H. 1987, *ApJ*, 318, 32
- Sijacki, D., Springel, V., & Haehnelt, M. G. 2011, *MNRAS*, 414, 3656
- Souza Lima, R., Mayer, L., Capelo, P. R., & Bellovary, J. M. 2016, *ArXiv e-prints*, arXiv:1610.01600
- Stone, J. M., & Norman, M. L. 1992, *ApJS*, 80, 753
- Whalen, D., & Norman, M. L. 2006, *ApJS*, 162, 281